Journal of Nano- and Electronic Physics
Vol. **14** No 2, 02014(5pp) (2022)

Журнал нано- та електронної фізики
Том **14** № 2, 02014(5cc) (2022)

Influence of Sulfur Incorporation on the Structural, Optical and Electrical Properties of Chemically Deposited ZnSe Thin Films

T.A.H. Mir[1], D.S. Patil[2], B.K. Sonawane[3,*]

[1] *Smt. G.G. Khadse College, Muktainagar, Jalgaon 425306 M.S, India*
[2] *Department of Electronics, School of Physical Sciences, Kavayitri Bahinabai Chaudhari North Maharashtra University, Jalgaon, 425001 M.S, India*
[3] *J.D.M.V.P. Co-Op. Samaj's Arts, Commerce and Science College, Jalgaon, 425001 M.S, India*

(Received 12 February 2022; revised manuscript received 26 April 2022; published online 29 April 2022)

The presented research aims to study the influence of sulfur incorporation on the optical, morphological, structural and electrical properties of chemically deposited zinc selenide thin films. The structural analysis reveals a peak shift of 0.47° of 2θ angle as the sulfur incorporation level increased from $x = 0$ (0 %) to $x = 0.3$ (15 %). The EDAX study shows that pure zinc selenide films are rich in selenium. With an increase in sulfur incorporation levels there is a continuous fall in selenium content. There is a significant reduction in variations in the range of grain sizes observed in SEM micrographs as the incorporation level increases. The transmittance is found to be higher in sulfur incorporated samples. The band gap energy is found to be increased from 2.63 to 3.17 eV with a rise in the sulfur incorporation level. An increase in the concentration of sulfur causes a rise in resistivity from 10^6 to 10^7 Ω·cm.

Keywords: Chemical bath deposition, Sulfur incorporation, Optical analysis, Electrical resistivity.

DOI: 10.21272/jnep.14(2).02014 PACS numbers: 73.61 Ga, 61.05.cp

1. INTRODUCTION

II-VI ternary alloys are gaining much attention compared to binary II-VI compounds due to their superior optical, structural and electrical properties. Ternary compounds can be prepared by incorporating a sufficient quantity of external elements in the parent compound to modulate the properties of nanomaterials retaining their large surface area. The availability of a large surface area is the requirement of thin-film solar cells. The cell efficiencies of 22.1 % and module efficiencies of 18.6 % are the significant achievements of CdTe thin-film solar cells [1]. CdS had dominated the solar cell industry for a long time. The use of *n*-CdS as a buffer layer was quite desirable with *p*-CdTe thin-film solar cells. But its toxicity made researchers look for the alternative in the form of ZnSe, ZnS, etc. [2, 3]. ZnSe, being non-toxic, wide band gap material, providing minimal lattice mismatch with Cu(In, Ga)Se_2 (CIGS) absorber, good transparency over the visible region [4, 5] can be suitable for use in solar cell applications. To facilitate the use of zinc selenide as a buffer layer in solar cell applications, it requires tunable band gaps and electrical properties. In the ternary materials like ZnS_xSe_{1-x}, by changing the composition of S and Se, the band gap can be modulated, and the blue response of the resultant films can be improved. This band gap modulation and blue response enhancement facilitate sulfur incorporated ZnSe thin films to explore its use as a buffer layer in CdTe and Cu(In, Ga)(S, $Se)_2$ (CIGSS) solar cells. Considering band gaps of ZnSe and ZnS, the ternary material ZnS_xSe_{1-x} offers a wider band gap in the range of 2.67 eV (ZnSe) to 3.67 eV (ZnS). Band gap tailoring is possible by varying the particle size by changing compositions of incorporated substance in the host, resulting in modifications in the electronic structure of the material. Band gap widening makes the material suitable to be used as a buffer layer in solar cell applications. Second, higher resistivity is desirable for a buffer layer as it resists impurities to enter in the absorber layer through the window layer, thus creating interface passivation [6, 7]. In this study, the promising zinc selenide host material is explored by adding sufficient quantity of sulfur to explore it in solar cell applications by modifying its optical and electrical properties like band gap and resistivity.

Different techniques were reported in the literature to prepare ZnS_xSe_{1-x} ternary alloy which include molecular beam epitaxy (MBE) [8], spray pyrolysis [9], thermal evaporation [10], electron beam evaporation [11], closed spaced evaporation [12], and chemical bath deposition (CBD) method [13, 14]. Most of the methods used sophisticated and expensive instrumentation with vacuum requirement and operated at higher temperatures. Among these, CBD acquires key features such as simplicity, low cost and ease in preparing films with a large surface area.

The method reported in this study is CBD for the preparation of ZnS_xSe_{1-x} ternary film. In the present investigation, the concentration of sulfur is varied in the ZnS_xSe_{1-x} film, and its effect on the structural, morphological, optical and electrical properties of sulfur incorporated zinc selenide thin films is studied and compared. In earlier studies [13, 14], chemical bath temperatures maintained for fabricating ZnSSe thin films on glass substrates were 70 and 80 °C, respectively. In this investigation, sulfur incorporated zinc selenide thin films were obtained at a relatively low temperature of 60 °C. However, all films were air annealed for two hours to improve crystallinity.

2. EXPERIMENTAL

The experimental process comprises three steps.

* b_ksonawane@rediffmail.com

Cleaning of the substrate is the first crucial step, which consists of immersing glass substrates for 12 h in dilute 5 % hydrochloric acid solution, rinsing it off with soapy water, and finally ultrasonic cleaning with deionized water for 15 min. In the second step, a stock solution of sodium selenosulphate (0.4 M) is prepared by refluxing 2.5 g of selenium powder with 7.5 g of sodium sulfite in 80 ml distilled water for 6 h at 85 °C with continuous stirring. The stock solution has to be prepared as Se powder cannot be used directly in the reaction as it does not dissolve in water easily, resulting in incomplete reaction. This ultimately causes Se residue formation in the final product which is quite difficult to be removed. Hence, a sodium selenosulfate stock is prepared and used as a source of Se. Due to early aging problem, sodium selenosulfate stock (Na_2SeSO_3) is used within two days and kept in an airtight container. The resultant stock solution is cooled overnight and stored after filtration. The deposition of thin films takes place in the third step by preparing a solution containing 10 ml of 0.5 M zinc sulfate monohydrate, a source of Zn^{2-}, 9 ml of hydrazine hydrate (80 %) as reducing agent and 7 ml of ammonia (25 %) as complexing agent. The volume of zinc sulfate monohydrate solution was kept fixed (10 ml) and volume of sodium selenosulfate as a source of Se^2 and thiourea as a source of S^{2-} were varied according to Table 1. The final volume of the bath is made up to 100 ml with deionized water and pH is maintained at 12. The deposition commences when fresh sodium selenosulfate is added to the prepared solution kept in a water bath, maintaining the temperature at 60 °C. The solution is stirred slowly throughout the reaction time of about 2 h. After deposition, the substrates were taken out and rinsed with deionized water to remove loosely attached particles on the substrate surface. This process was repeated for different concentrations of sulfur ($x = 0$ (0 %), 0.1 (5 %), 0.2 (10 %) and 0.3 (15 %)). All the films were annealed further at 200 °C in air for 2 h in order to improve crystallinity.

X-ray diffraction analysis of ZnS_xSe_{1-x} thin films was done by an X-ray diffractometer Philips PW3710 ($\lambda = 1.54056$ Å) in the range of 2θ from 200-700 with CuKα radiation. Morphological and elemental analysis of thin films was performed on a Scanning Electron Microscope (JEOL JED-2300 JAPAN) with an EDAX (energy-dispersive X-ray spectroscopy) facility. The optical transmission spectra of ZnS_xSe_{1-x} films were obtained by a Spectrophotometer (UV-3600 SHIMADZU) in the spectral range 350-800 nm. The electrical resistivity of pure and sulfur incorporated zinc selenide thin films with various incorporation levels was measured with a dc two-probe method. Silver paste was glued at 1 cm apart on thin films for contact purpose. The temperature range of 300 K-425 K was maintained. The current measurement was done with a pico ammeter.

3. RESULTS AND DISCUSSION

3.1 Structural Characterization

Zinc selenide exhibits two structural phases, namely hexagonal wurtzite and cubic zinc blende or sometimes a mixture of both [4]. In this report, a pure zinc selenide thin film ($x = 0$) exhibits well-resolved peaks at 27.33°, and weak peaks at 45.28° and 54.36° of 2θ, as shown in Fig. 1a. These peaks are attributed to the (111), (220) and (311) planes, respectively, with a preferred orientation in the (111) direction. This cubic phase was confirmed by JCPDS data file No. 80-0021. A few impurity peaks are visible in the XRD graphs. As shown in Fig. 1b, there is a peak shift of 0.47° at peak positions of (111) towards the higher 2θ angle from 27.33° to 28.5° as the sulfur incorporation level increases from $x = 0$ to $x = 0.3$. The reason behind this shift may be the size difference in the atomic radius of S (1.09 Å) and Se (1.22 Å) and variations in the lattice parameters [11, 15].

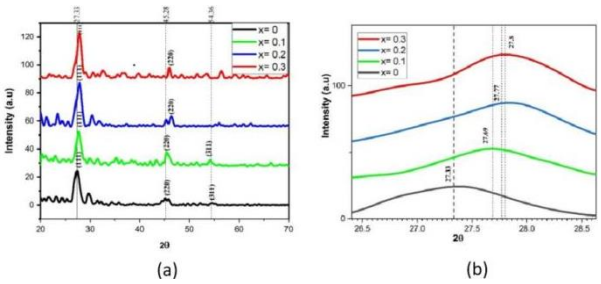

Fig. 1 – (a) XRD analysis and (b) enlarged peak (111) of pure and sulfur incorporated zinc selenide thin films at various concentration of sulfur (x)

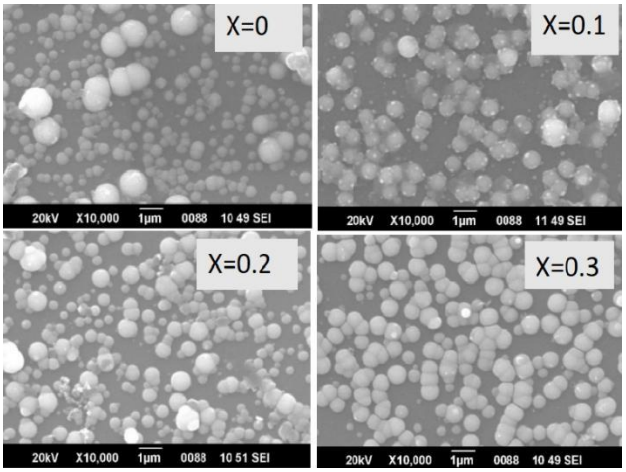

Fig. 2 – Surface morphology of pure and sulfur incorporated zinc selenide thin films at various concentrations of sulfur (x)

The data obtained from XRD analysis of sulfur incorporated and pure samples such as FWHM (full width at half maximum) and d spacing of the prominent peak are listed in Table 2.

The Debye-Scherrer formula was used to calculate the average crystallite size (D) of all sulfur incorporated and pure ZnSe thin films by considering the (111) diffraction peak:

$$D = \frac{0.94\lambda}{\beta\cos\theta},$$

where β is the FWHM of the prominent peak (111), λ is the wavelength of the diffraction source and θ is the Bragg angle. The obtained values of the crystallite size lie in the range of 6.85-9.55 nm.

The interplanar spacing (d) was estimated by using the Bragg relation:

Table 1 –Volumetric quantities for a solution of ZnS_xSe_{1-x} thin films

Concentration of sulfur (x)	2θ (deg.)	Planes (hkl)	FWHM β (rad)	d (Å)
0	27.33	111	0.021	3.2647
0.1	27.69	111	0.019	3.2231
0.2	27.77	111	0.018	3.2140
0.3	27.80	111	0.015	3.2106

$$d = \frac{\lambda}{2\sin\theta}.$$

As the obtained films exhibit a cubic structure, the lattice parameter (a) was calculated by the following relation:

$$\frac{1}{d^2} = \frac{h^2 + k^2 + l^2}{a^2}.$$

Here, h, k, l are the lattice planes. The dislocation density was calculated using the following relation:

$$\delta = \frac{15\beta\cos\theta}{4aD}.$$

The strain (ε) in the films was calculated from the relation

$$\varepsilon = \frac{\beta\cos\theta}{4}.$$

The grain size, lattice parameter, strain and dislocation density of pure and sulfur incorporated films are summarized in Table 3. The dislocation density and strain are found to decrease with a rise in sulfur content in the films, indicating an improvement in crystallinity. The grain size is observed to increase from 6.85 to 9.55 nm with a rise in sulfur concentration. SEM analysis also supports the XRD results of the study.

3.2 Elemental and Morphological Characterization

The elemental study of pure and sulfur incorporated zinc selenide thin films is given in Table 4. It is observed that all films are rich in selenium. A continuous trend of reduction of Se is observed with an increase in the amount of sulfur in the films which is expected.

The SEM images of pure and sulfur incorporated zinc selenide thin films at various concentrations of sulfur are presented in Fig. 2. It is worth noting that the micrograph of pure zinc selenide thin film ($x = 0$) contains a blend of tiny and enlarged spherical nanoparticles covering the entire surface of the glass substrate. For the concentration $x = 0.1$, spherical-shaped nanoparticles were seen developing minute structures all over them, however, larger voids being visible. The obtained range of grain sizes in the SEM micrograph is few nanometers to hundreds of nanometers. It is worth noting that this variation in grain size is reduced as concentration of sulfur increased and for $x = 0.3$, there is seen significant uniformity of grain sizes.

Table 2 – XRD data analysis of and sulfur incorporated zinc selenide thin films at various concentrations of sulfur (x)

Composition	Samples	Zinc sulfate	Sodium selenosulfate	Thiourea
x	ZnS_xSe_{1-x} solution (ml)	solution (ml)	solution (ml)	solution (ml)
0	ZnSe	10	20	0
0.1	$ZnS_{0.1}Se_{0.9}$	10	18	2
0.2	$ZnS_{0.2}Se_{0.8}$	10	16	4
0.3	$ZnS_{0.3}Se_{0.7}$	10	14	6

Table 3 – Grain size, lattice parameter, strain and dislocation density of pure and sulfur incorporated zinc selenide thin films at various concentrations of sulfur (x)

x	Grain size (nm)	Lattice parameter (Å)	Strain $(\text{lin}^{-2}\,\text{m}^{-4}) \times 10^{-3}$	Dislocation density $(10^{16}/\text{m}^2)$
0	6.85	5.6547	5.28	2.13
0.1	7.72	5.5826	4.68	1.68
0.2	8.15	5.5668	4.43	1.50
0.3	9.55	5.5609	3.77	1.09

Table 4 – Elemental analysis of pure and sulfur incorporated zinc selenide thin films at various concentrations of sulfur (x)

x	0	0.1	0.2	0.3
Zn (at. %)	34.53	43.58	40.30	40.69
Se (at. %)	65.47	50.53	49.34	44.15
S (at. %)	0	5.89	10.36	15.16

3.3 Optical Characterization

The sulfur incorporated zinc selenide thin films exhibit higher transmittance than the pure film, as depicted in the transmittance spectra in Fig. 3. The high transmittance plays a vital role in the use of thin films as a buffer layer in solar cell applications [16]. The transition from the valence band to the conduction band is given by the fundamental absorption depicted by the following relation and it helps to find out the band gap of the films. The band gap was obtained using the following relation [17]:

$$\alpha = A\frac{(h\nu - Eg)^n}{h\upsilon},$$

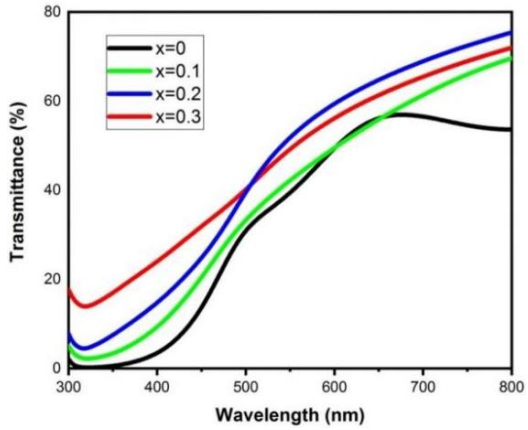

Fig. 3 – Transmittance spectra of pure and sulfur incorporated zinc selenide thin films with various concentrations of sulfur (x)

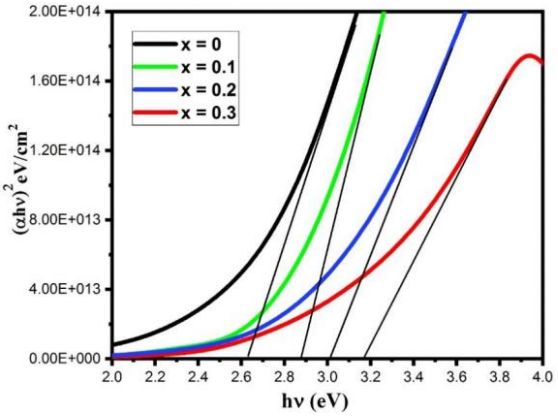

Fig. 4 –Plot of $(\alpha hv)^2$ versus photon energy (hv) of pure and sulfur incorporated zinc selenide thin films

where α is the absorption coefficient, A is a constant, n is equal to 1/2 for a direct band gap semiconductor. The energy intercept of the plot $(\alpha hv)^2$ versus hv, as shown in Fig. 4, gives the band gap for the direct transition. The band gap energy of ZnSe is 2.67 eV and of ZnS is 3.67 eV, hence the band gap of sulfur incorporated zinc selenide thin films is found to increase from 2.63 eV to 3.17 eV as sulfur concentration is raised from $x = 0$ (0 %) to $x = 0.3$ (15 %) in our study. Thus, the band gap of sulfur incorporated zinc selenide thin films increases with an increase in the concentration of sulfur content in the film. Similar observations were reported elsewhere [18].

3.4 Electrical Characterization

The variation of electrical resistivity with temperature during cooling for various concentrations of sulfur are presented in Fig. 5. At room temperature, the resistivity values increase from 106 to 107 Ω·cm as concentration of sulfur increases from $x = 0$ (0 %) to $x = 0.3$ (15 %) respectively. From the graph, it is evident that resistivity decreases with an increase in temperature, confirming the semiconducting nature. It is worth noting that the rise in the sulfur concentration causes an increase in resistivity of thin films. Thus, fall in selenium content and rise in sulfur content in the films increase film resistivity. This behavior is observed in the literature [14].

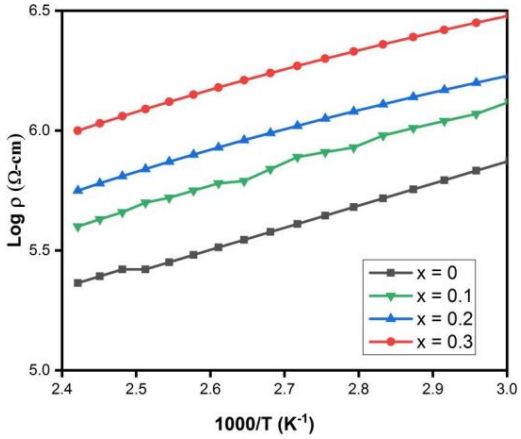

Fig. 5 – Variation of $\log\rho$ with $1000/T$ for pure and sulfur incorporated zinc selenide thin films with various sulfur concentrations

4. CONCLUSIONS

Sulphur incorporated zinc selenide thin films have been synthesized by a convenient chemical bath deposition method for various sulfur concentrations. XRD studies revealed a peak shift towards higher angles 2θ with increasing sulfur concentrations. EDAX studies confirmed the replacement of selenium atoms by sulfur atoms with an increase in sulfur concentrations. The electrical resistivity was found to be increased from10^6 to 10^7 Ωcm with the increase in concentration of sulfur. An increase in bandgap energy is observed from 2.63 to 3.17 eV as sulfur content increases in the films. Thus, the wider band gap, higher transmittance and moderately high resistivity of sulfur incorporated ZnSe thin films can find their place in solar cell applications.

REFERENCES

1. M.A. Green, K. Emery, Y. Hishikawa, W. Warta, E.D. Dunlop, D.H. Levi, A.W.Y. Ho-Baillie, *Prog. Photovolt.: Res. Appl.* **25**, 333 (2017).
2. A. Ennaoui, S. Siebentritt, M. Ch. Lux-Steiner, W. Riedl, F. Karg, *Sol. Energ. Mater. Sol. C.* **67**, 31 (2001).
3. B.R. Sankapal, S.D. Sartale, C.D. Lokhande, A. Ennaoui, *Sol. Energ. Mater. Sol. C* **83**, 447 (2004).
4. C.D. Lokhande, P.S. Patil, H. Tributsch, A. Ennaou, *Sol. Energ. Mater. Sol. C* **55**, 379 (1998).
5. A. Rumberg, Ch. Sommerhalter, M. Toplak, A. Jager-Waldau, M. Lux-Steiner, *Thin Solid Films* **361**, 172 (2000).
6. L.M. Caicedo, G. Cediel, A. Dussan, J.W. Sandino, C. Calderon, G. Gordillo, *phys. status solidi b* **220**, 249 (2000).
7. G. Gordillo, C. Calderon, H. Infante, *Twenty-Ninth IEEE Photovoltaic Specialists Conference*, 644 (New Orleans, USA: IEEE: 2002).
8. H.J. Kim, B.J. Kim, T.W. Kim, K.H. Yoo, *Appl. Surf. Sci.* **255**, 5048 (2009).
9. S. Fridjine, S. Touihri, K. Boubaker, M. Amlouk, *J. Cryst. Growth* **312**, 202 (2010).
10. S. Park, H. Kim, C. Jin, C. Lee, *Curr. Appl. Phys.* **12**, 499 (2012).
11. K.M.M. Abo-Hassan, M.R. Muhamad, S. Radhakrishna,

Physica B **358**, 256 (2005).
12. Y.P. Venkata Subbaiah, P. Prathap, K.T.R. Reddy, D. Mangalaraj, K. Kim, J. Yi, *J. Phys. D: Appl. Phys.* **40**, 3683 (2007).
13. J. Liu, A.X. Wei, M.X. Zhuang, Y. Zhao, *J. Mater. Sci. Mater. El.* **24**, 1348 (2013).
14. H.K. Sadekar, A.V. Ghule, R. Sharma, *J. Alloy. Compd.* **509**, 5525 (2011).
15. R. Shaaban, A. Almohammedi, G.A. Ali, K.F. Chong, A. Adel, A. Ashour, *Optik* **164**, 527 (2018).
16. E.R. Sharma, S.L. Patel, S. Chander, M.D. Kannan, M.S. Dhaka, *Phys. Lett. A* **384**, 126097 (2020).
17. K.M. Garadkar, A.A. Patil, P.P. Hankare, P.A. Chate, D.J. Sathe, S.D. Delekar, *J. Alloy. Compd.* **487**, 786 (2009).
18. C. Dhanemozhi, R. John, K.R. Murali, *Mater. Today. Proc.* **4**, 5185 (2017).

Вплив включення сірки на структурні, оптичні та електричні властивості хімічно осаджених тонких плівок ZnSe

T.A.H. Mir[1], D.S. Patil[2], B.K. Sonawane[3]

[1] *Smt. G.G. Khadse College, Muktainagar, Jalgaon 425306 M.S, India*
[2] *Department of Electronics, School of Physical Sciences, Kavayitri Bahinabai Chaudhari North Maharashtra University, Jalgaon, 425001 M.S, India*
[3] *J.D.M.V.P. Co-Op. Samaj's Arts, Commerce and Science College, Jalgaon, 425001 M.S, India*

Метою представленого дослідження є вивчення впливу включення сірки на оптичні, морфологічні, структурні та електричні властивості хімічно осаджених тонких плівок селеніду цинку. Структурний аналіз показує зсув піку на 0.47°, оскільки рівень включення сірки підвищився з $x = 0$ (0 %) до $x = 0.3$ (15 %). Дослідження EDAX виявляє, що плівки чистого селеніду цинку багаті селеном. Зі збільшенням рівня включення сірки відбувається безперервне зниження вмісту селену. На мікрофотографіях SEM спостерігається значне зменшення коливань діапазону розмірів зерен із збільшенням рівня включення сірки. Виявлено, що коефіцієнт пропускання вищий у зразках із включеннями сірки. Встановлено, що енергія забороненої зони збільшується з 2,63 до 3,17 еВ із збільшенням рівня включення сірки. Збільшення концентрації сірки викликає підвищення питомого опору від 10^6 до 10^7 Ом·см.

Ключові слова: Хімічне осадження у ванні, Включення сірки, Оптичний аналіз, Питомий електричний опір.